Shuo Wang
Key Laboratory of Education Ministry for Modern Design and Rotor-Bearing System,
School of Mechanical Engineering,
Xi'an Jiaotong University,
Xi'an 710049, China
e-mail: wstyxjtu@163.com

Tonghai Wu[1]
Key Laboratory of Education Ministry for Modern Design and Rotor-Bearing System,
School of Mechanical Engineering,
Xi'an Jiaotong University,
Xi'an 710049, China
e-mail: wt-h@163.com

Kunpeng Wang
Key Laboratory of Education Ministry for Modern Design and Rotor-Bearing System,
School of Mechanical Engineering,
Xi'an Jiaotong University,
Xi'an 710049, China
e-mail: moyuansuishang@163.com

Thompson Sarkodie-Gyan
Laboratory for Industrial Metrology and Automation,
Department of Electrical and Computer Engineering,
University of Texas at El Paso,
El Paso, TX 79968
e-mail: tsarkodi@utep.edu

Ferrograph Analysis With Improved Particle Segmentation and Classification Methods

Ferrograph analysis has been adopted over decades for determining the root causes of ongoing wear faults. After decades of manual operation, this traditional technique is being driven by intelligent algorithms for automatic identification of wear debris. However, the accuracy and robustness of this algorithm remain marginalized when applied in industries due to various types and color blurry of particles. To address this issue, this paper introduces an automatic ferrograph analysis model with a segmentation method and a two-level classification strategy. In order to obtain wear particles from the color ferrograph image, an adaptive Otsu threshold is adopted in three channel images to solve the color blurry in particle segmentation. By grouping particle parameters into shape and morphology ones, a two-level identification strategy is proposed. The first one is to classify rubbing, cutting, and spherical particles, referring to the fuzzy approach degree of shape parameters. In the second level, the shape-close particles are classified with imperceptible textures and back propagation neural network (BPNN). These objective parameters are constructed by applying the principal component analysis into seven texture features and inputted into a BPNN-based model to classify fatigue and severe sliding particles. In order to train the BPNN, more than 100 ferrograph images are sampled together, whereby standard ferrograph analysis is performed on the particle identification. The performance of the identification exhibits an accuracy exceeding 90% for rubbing, cutting, and spherical particles, whereas about 80% accuracy has been registered for both severe sliding and fatigue particles. [DOI: 10.1115/1.4045291]

Keywords: artificial intelligence, machine learning for engineering applications

1 Introduction

Wear-induced failure of key equipment is the focus of condition monitoring for many industrial enterprises, the petrochemical industry is an obvious example of this category. To avoid such failure in the operating equipment, ferrography technique is widely adopted to evaluate the mechanism and severity of wear via the particles carried by the cycling lubricant [1–3]. Over decades, ferrograph analysis has been manually carried out and empirically on particle image segmentation and identification, which is time-consuming and costly [4,5]. To address this issue, a vast contribution of algorithms has been reported for ferrograph image identification [4], but their accuracy and robustness remain marginalized when applied in industries. The interference inherent in the low contrasts and blurry occurrences of particle images might be as a result of the marginalized accuracy that could have been overseen during the initial recognition strategies. Consequently, there is a great demand for improving the performance of this promising technique through the automation of particle image segmentation and classification.

Particle segmentation from ferrograph images is the foundation of automated ferrograph analysis. As a contribution to this notion, many segmentation methods that involve particle morphological characteristics are reported with different strategies [6,7]. In particular, researchers tend to adopt a C-V model to extract wear particle contours, even though this method divides the particle into many small areas [8]. Nevertheless, there arises an enormous amount of particles in a single image. This occurrence may lead to some unacceptable low rates in efficiency of the one-by-one segmentation. Furthermore, adaptive methods are adopted to extract complete wear particles from the background with a k-means or a watershed and ant colony-based clustering algorithm [7,9], but these methods are very sensitive to the color of particles that leads to the highly false segmentation when there are particles in dark, light, or even in mixed colors.

The main challenge for the particle identification lies in the fact that there are large numbers of typical particles, and they have various features both in color and in morphology. Correspondingly, the algorithms for automatic classification should be sufficiently intelligent in any situation. Wear particle identification systems have been established with different algorithms [10–12]. Representatively, with shape features extracted by image processing, a new radial concave deviation (RCD) method is developed to identify regular, elongated, spherical, and irregular particles [13]. Similar to the RCD method, an automated identification model is constructed by inputting particle morphological characteristics into a feed-forward neural network [14]. In actual fact, there exist over 200 morphological features that contribute toward the description of particles [15]. These characteristics are capable toward the introduction of the relevant features and redundant information data for the classification of the different particle types. In response to these demands, further work has been carried out on extracting integrated features by a GP-based evolutionary method. The GP evolved features are adopted to train a support vector machine (SVM) classifier to identify sliding, cutting, and oxidative particles [16]. Meanwhile, a multivariate discrimination method is developed through the decision tree to classify cutting, fatigue, slight sliding, and severe sliding particles [17]. These methods provide good ideas to classify wear particles in distinguishable shape characteristics, which facilitate the automatic recognition of wear types.

With respect to the effect, the classification of the particles of the severe sliding and fatigue types seems to be a big task because the

[1]Corresponding author.

Manuscript received June 17, 2019; final manuscript received October 16, 2019; published online October 25, 2019. Assoc. Editor: Ying Liu.

discrimination relays on the faint surface textures. Earlier researchers use gray-level co-occurrence matrix (GLCM) to acquire texture characteristics from wear particle surfaces and then make identification of these two particles through an integrated algorithm of principal component analysis (PCA) and gray correlation [15]. However, the GLCM textures can only represent the relation between image pixels, but they are unable to comprehensively characterize particle surfaces. The solution is directed to another way by improving the resolution of particle features; laser scanning confocal microscopy [18] and atomic force microscopy [19] are used for extracting 3D features such as thickness and surface roughness. In order to identify the severe sliding and fatigue particles, these aforementioned features serve as inputs into the SVM-based [19] or the BPNN models [20], respectively. These suggested methodologies seem to provide extensive morphological information as opposed to the conventional two-dimensional (2D) approaches. They also exhibit absolute improvements toward the accuracy of the identification of the particle type. However, the complexities involved in the operation of these instruments, and coupled with their high costs, make their application in the industry greatly marginalized.

Although current analytic methodologies have gained certain successes in particle segmentation and classification, yet still, they are insufficient in meeting the demand of the petrochemical industry. To address this issue, we developed an automated ferrograph to identify typical wear particles from captured ferrograph images. In order to deal with wear particle images in different situations, three channel images are selected and dealt with the adaptive Otsu method to segment wear particles in dark color, light color, or mixed color from the background. After the acquisition of morphological features, the fuzzy inference is applied to distinguish the rubbing, spherical, and cutting particles which are easy to be identified. The PCA methodology is preferred for the extraction of the comprehensive texture parameters toward the characterization of the severe sliding and fatigue particles, and then, a BPNN model is constructed to identify them. With this framework, an automated identification system is established for typical wear particles. Its performance may be estimated by the application of actual particles. This experimental investigation offers an insight into the rate of the efficiency in the solution toward the automation of the particle classification. This procedure may contribute toward enhancing the analysis of machine wear state.

The rest of this paper includes four sections: Sec. 2 depicts an adaptive particle image segmentation; The particle identification strategy and the corresponding verification are given in Sec. 3; Secs. 4 and 5 describe the discussions and the conclusions.

2 Adaptive Segmentation for Wear Particle Image

Particles segmentation from ferrograph images is the basis of the characteristics extraction for the following automated type recognition. However, the particles collected from petrochemical equipment always have dark, light, or mixed colors in captured images, as shown in Fig. 1. The different particle images result in that part of the particle area may be lost when they are segmented. Therefore, it becomes of ultimate significance to construct an adaptive segmentation method for ferrograph images.

2.1 Particle Image Segmentation Method. With respect to Fig. 1, there exist discrepancies between the particles and their respective backgrounds on the ferrograph images, notwithstanding the fact that the color of the particles may be different. In this case, a suitable threshold may be estimated toward the segmentation of the particles from the background. Applying the least square method, the Otsu method is capable of adaptively choosing an optimal segmentation threshold from the distribution of the image gray level [21]. This method can greatly reduce the search time for computing the segmentation threshold due to its optimization processing.

Fig. 1 Original wear particle image

Therefore, the Otsu method is adopted to deal with ferrograph images with the following procedures [2].

Otsu adopts threshold k to segment gray images. The gray scale image from 0 to k is segmented into particle parts M_0, whereas the rest of the zone (gray scale from $k+1$ to $l-1$) is estimated as the background M_1. The variance between M_0 and M_1 can be considered as a measure of uniformity of the gray distribution. The greater the variance between the particle and background, the greater the difference between the two parts of the image, that is, the better the particle image segmentation. The class variance $\sigma^2(k)$ can be estimated through Eqs. (1) and (2).

$$\begin{cases} \omega_0 = \sum_{i=0}^{k} \dfrac{n_i}{N} & \mu_0 = \sum_{i=0}^{k} \dfrac{i^* n_i}{\omega_0 * N} \\ \omega_1 = \sum_{i=k+1}^{l-1} \dfrac{n_i}{N} & \mu_1 = \sum_{i=k+1}^{l-1} \dfrac{i^* n_i}{\omega_1 * N} \end{cases} \tag{1}$$

$$\sigma^2(k) = \omega_0 \omega_1 (\mu_0 - \mu_1)^2 \tag{2}$$

where N is the pixel number of the gray image, n_i is the pixel number of the ith gray level in the image, ω_0 is the proportion of the particles, μ_0 is the average gray level of particles, ω_1 is the proportion of the background, and μ_1 is the average gray level of background.

The optimal threshold k^* may be obtained through the traversion of the gray scales from 0 to $l-1$, whereby the pixel points in the image may be classified into the particle and the background regions, respectively. Hereby, the black zones represent wear particles, and the background is the white zones.

2.2 Different Channel Image Analysis. Aiming at segmenting the three situations of particle images, four channel images are obtained by transforming the original RGB color space to HSV color space [22], including gray image, H, S, and V channel image. The four channel images are segmented with the Otsu threshold method, as illustrated in Fig. 2. As may be observed, HSV color space describes the particle image from three perspectives (brightness, saturation, and hue), and the three images are quite different from the original image. It can be found from the segmentation results that the V channel image is suitable for the dark particle image segmentation, while the small dark particles and the large light particles are segmented from the S channel image. However, neither the small dark particles nor the large light particles are effectively segmented from the H channel image. In addition, Fig. 2(*e*) shows that light-colored wear particles can be effectively segmented, while dark-colored wear particles cannot be segmented from the gray image.

The number of pixels in the wear particle area is counted for each channel segmentation image, as shown in Fig. 3. Combined with Figs. 2 and 3, some rules may be concluded: the S-channel-based segmentation can obtain the complete wear particle because of

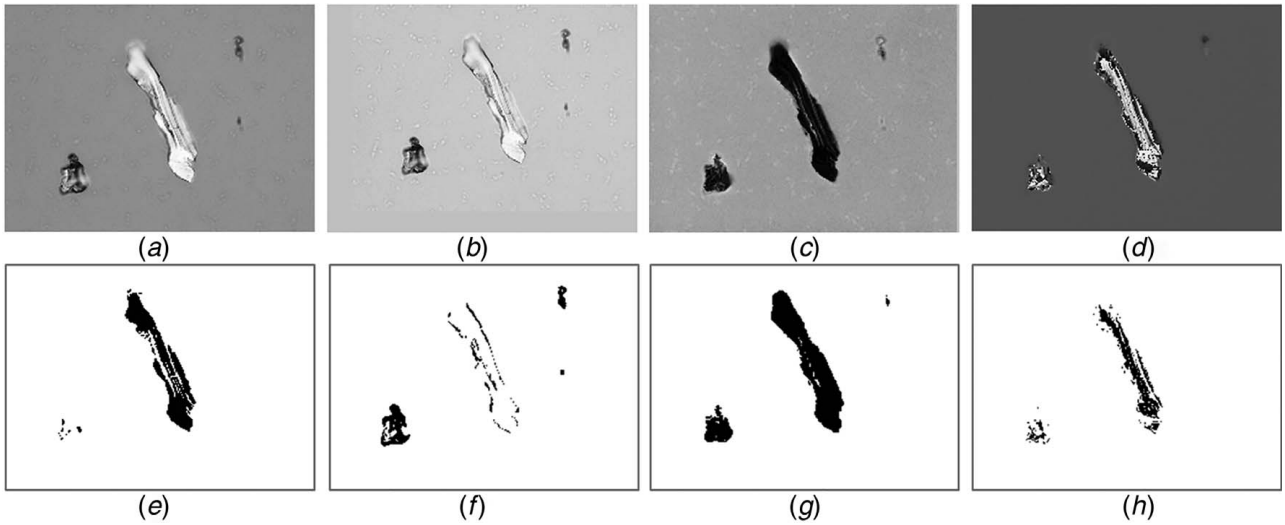

Fig. 2 Image segmentation result based on RGB and HSV color space: (*a*) gray image, (*b*) V-channel gray image, (*c*) S-channel image, (*d*) H-channel image, (*e*) gray-image segmentation, (*f*) V-channel gray image segmentation, (*g*) S-channel image segmentation, and (*h*) H-channel image segmentation

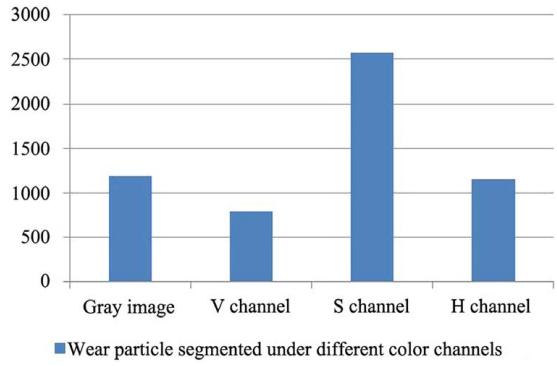

Fig. 3 Area comparison of wear particle segmented under different color channels

the largest area (reaching 2571); the smallest particle area is 793 segmented based on V-component image, which can reflect the small dark wear particles; The wear particle area segmented based on RGB gray image reaches 1188, which is the area of light-color wear particle image.

In summary, the gray-image-based segmentation method can distinguish light-color particles, the V-channel-based segmentation method can segment dark-color particles, and the S-channel-based segmentation method can simultaneously extract both dark and light wear particles from the background. Therefore, different dark-color and light-color wear particles can be segmented with choosing gray image, V-channel image, or S-channel image. Furthermore, the open operation, closed operation, and connected region marking algorithm are introduced to achieve an accurate and effective segmentation for various particle images. Part of segmentation results are shown in Fig. 4.

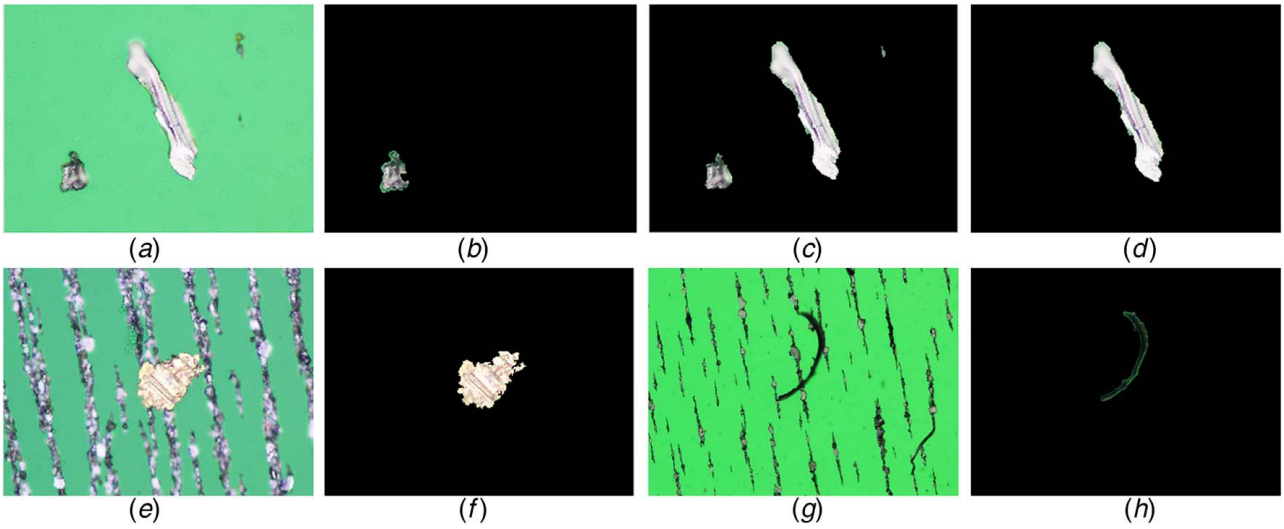

Fig. 4 Segmented results of various wear debris images: (*a*) original mixed-color particle image, (*b*) segmentation of dark-color particle from (*a*), (*c*) co-segmentation of dark-color and light-color particles from (*a*), (*d*) segmentation of light-color particle from (*a*), (*e*) original image of particle in the chain, (*f*) segmentation of particle from (*e*), (*g*) original image of particle in the chain, and (*h*) segmentation of particle from (*f*)

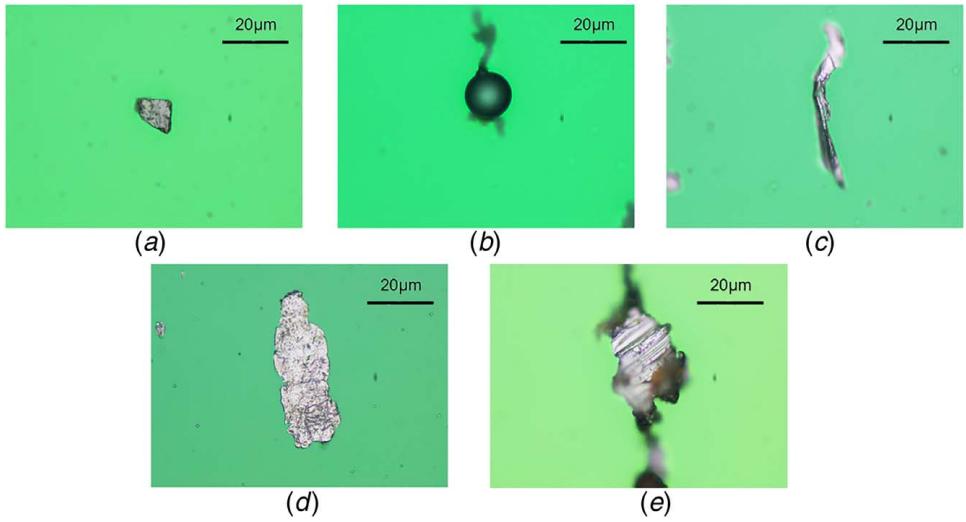

Fig. 5 Images of different types of particles

Table 1 Generation mechanisms of wear particles [1,12,13,15]

Type	Features	Generation mechanism	Possible wear state
Rubbing	Thin and its size in 0.5–15 μm	The frictional component of the failure of the shear mixing layers	The occurrence of failure with dramatic increase in the particle number
Cutting	Long particles	Hard particles penetrating the soft surfaces	Impending trouble of severe cutting wear
Spherical	Ball-like particles	The grinding of the cracks or melting of metals at high temperatures	The precursor of early pitting or severe wear
Serious sliding	Parallel scratches on surface	Excessive stress on the surface	The damage of oil film
Fatigue	Smooth surfaces with pitting	Pitting after surface fatigue	Heavy load or over-speed

3 Wear Particle Recognition Based on Fuzzy Inference and BPNN

Wear particle recognition is the core of wear debris analysis (WDA) technology, but traditional particle classification mainly relies on experts or experienced analysts. In order to address this issue, classification methodology based on a two-level approach is constructed with the shape and texture features of five typical particles in this section.

3.1 Wear Particle Recognition Strategy. The morphological features inherent in the wear particles that include shape and texture, exhibit some amount of closeness toward the connection with the generation mechanism of the particles and the running state of the equipment. Some research work has been carried out to systematically analyze wear particle types, mainly involving rubbing, cutting, spherical, severe sliding, and fatigue particles. Different types of particles have typical shapes, edges, and surface textures which correspond to its generation mechanisms. The shapes of typical particles are shown in Fig. 5. The connectivity of the morphological features of the particles and the running state of the machines is illustrated in Table 1 [1,12,13,15].

As may be observed from Fig. 5, rubbing, spherical, and cutting particles have distinct shape characteristics—rubbing particles have a smaller size, spherical particles are ball-like, and cutting particles are spiral and arc. In this manner, these particles may be accurately classified with 2D shape features. However, the fatigue and severe sliding wear particles have high similarities on the shape and color characteristics, which lead to low-identification accuracy of these two kinds of particles. To address this issue, a two-level identification strategy is developed as follows:

(1) The rubbing, spherical, and cutting wear particles are first distinguished by combining the three characteristic parameters (area, roundness, and aspect ratio) with fuzzy inference.
(2) The application of the PCA enables the extraction of comprehensive texture parameters from the GLCM parameters and Tamura texture parameters. Furthermore, a BPNN-based model is constructed for the fatigue and severe sliding particle classification.

The specific process framework is shown in Fig. 6.

3.2 First-Level Classification for Four Typical Particles. Various wear particles exist in lubricating oil, and their shapes and textures are different, even for the same type of wear particles. This will lead to a fuzzy for wear particle identification. The fuzzy degree between two wear particles can be described with fuzzy inference [23,24]. Therefore, the fuzzy inference method is applied for the recognition of the type of particles through comparing the identified particles with the standard particle model.

Based on the strategy involving the particle recognition, rubbing, cutting, and spherical wear particles are first recognized with the area, roundness, and aspect ratio, and the remaining two kinds of particles are then being identified in the following sections. The ambiguity domain (U) of fuzzy inference can be defined as: $U=\{$rubbing particle ($\tilde{A}_1$), cutting particle ($\tilde{A}_2$), spherical particle ($\tilde{A}_3$), other particles ($\tilde{A}_4$)$\}$, and $X=\{$area (X_1), roundness (X_2), aspect ratio (X_3)$\}$ are selected as the description index, whereby the other particles represent fatigue and severe sliding particles. Particle fuzzy sets are calculated by normalizing the characteristic parameters in Table 2 in Ref. [17], which are extracted from various wear particles in the sample library.

Fuzzy inference method can comprehensively identify the target through the evaluation of multiple factors. Due to the same trend in the predicted results of different closeness [25], the maximum–minimum degree approach is applied to calculate the attribution

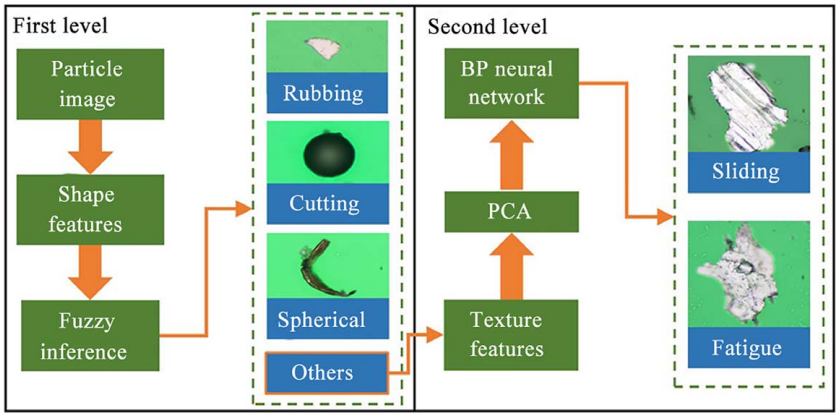

Fig. 6 Flowchart of wear particle recognition based on fuzzy proximity and BPNN

Table 2 Characteristics of wear particles in the sample base

Parameter	$\tilde{A}_1$	$\tilde{A}_2$	$\tilde{A}_3$	$\tilde{A}_4$
A_1	0.0266	0.1671	0.0819	0.3347
A_2	0.6874	0.0912	0.9165	0.6470
A_3	0.0187	0.3986	0.0026	0.0264

degree of particles to be tested and sample particles.

$$\sigma_0(\tilde{A}_j, \tilde{B}) = \frac{2^* \sum_{i=1}^{3} (\tilde{A}_j(x_i) \wedge \tilde{B}(x_i))}{\sum_{i=1}^{3} (\tilde{A}_j(x_i) + \tilde{B}(x_i))}, \quad (j = 1, 2, 3, 4, 5) \tag{3}$$

where $\tilde{A}_j(x_i)$ and $\tilde{B}(x_i)$ are the ith eigenvalue of particle A in type j in Sample base and tested particle B, respectively.

According to the proximity principle, if $\sigma_0(\tilde{A}_{i_0}, \tilde{B}) = \bigvee_{k=1}^{m} \sigma_0(\tilde{A}_k, \tilde{B})$, $\tilde{B}$ is classified into type $\tilde{A}_{i_0}$. In this way, the type of particles can be determined with the attributive degree.

3.3 Second-Level Classification for Fatigue and Severe Sliding Particle. Even though there are distinct texture differences between the surfaces of severe sliding and fatigue particles, the recognition rate of these two particles is still very low due to the fact that the extracted texture parameters cannot effectively characterize wear particles. To address this issue, two steps are involved including (1) comprehensive texture extraction based on PCA and (2) BPNN-based particle identification model.

3.3.1 Comprehensive Texture Extraction Based on Principal Component Analysis. The significant dissimilarities of the severe sliding and fatigue particles exist on the surface textures. GLCM textures and Tamura textures provide a reliable means for texture extraction. GLCM can describe the change rule of image pixels with a set of parameters [26], such as energy, inertia, correlation, and entropy. Tamura method can extract texture features from the perspective of human subjective psychology [27] and its texture features (roughness, contrast, and orientation) match human visual perception. The definition of these parameters is described in Table 3.

Coming from two models, the seven texture parameters may include relevant information. If these parameters are directly adopted to characterize a surface texture, the redundant texture features may result in a low recognition rate. Hence, statistical texture features need to be extracted to reduce variables without losing key information. As an effective dimension reduction method, PCA can convert a group of original data vectors into fewer integrated data vectors which are not correlated with each other [28,29]. The PCA method has been adopted toward the estimation of the statistical texture parameters from the seven parameters, and the results are shown in Table 4. It may be recorded that the cumulative contribution rate of the first three principal components has reached 87.7896% (exceeding 85%). Therefore, the feature vectors corresponding to the eigenvalues of 4.2468, 1.223, and 0.6755 are selected as the comprehensive textures.

Table 3 Texture parameters from GLCM and Tamura model

Parameters	Definition
Energy	The square of the sum of element values of GLCM.
Inertia	The quadratic statistics of GLCM, representing surface details.
Relevance	The reflection of certain gray value extending along a certain direction.
Entropy	The uniformity of pixel distribution in gray-scale images.
Roughness	The representation of the small spacing or unevenness of peak-valley on particle surfaces.
Contrast	The brightness level between the brightest pixel and the darkest pixel in the image area.
Roughness	The arrangement consistency of texture along a certain direction in an image.

3.3.2 BPNN-Based Particle Identification Model. An appropriate selection of intelligent algorithm can facilitate the fatigue and severe sliding particle identification. The common-used identification methodologies include SVM [19], BPNN [30], and recurrent neural networks (RNN) [31]. SVM is a binary classifier developed on the statistical learning theory, and its learning ability and generalization ability depend on the kernel function. However, it is difficult to construct an effective kernel function for particle identification because of the complex textures of severe sliding and fatigue particle images. BPNN, a multi-layer feed-forward neural network, can fully reveal complex nonlinear relations with its strong learning ability [30]. RNN can achieve a classification based on dynamic signals in the serialized data, but the introduction of historical information makes its

Table 4 Statistical texture parameters of typical particles in sample base

Principal component	Eigen value	Contribution rate	Accumulated contribution rate
First	4.2468	60.6685%	60.6685%
Second	1.2230	17.4710%	78.1395%
Third	0.6755	9.6501%	87.7896%

Table 5 The output of BPNN classifier

Output	Output 01	Output 02
Fatigue	1	0
Severe sliding	1	0

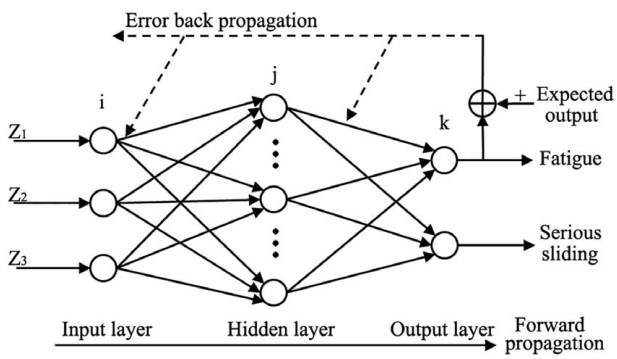

Fig. 7 BPNN-based wear particle classifier

computational complexity far beyond BPNN. On account of this procedure, the BPNN is applied toward the construction of the particle classifier: the comprehensive texture parameters extracted by PCA are selected as the input; a modification of the structure of the BPNN-based model is performed using the input parameters; the output of model includes two types whereas the final particle type is determined using Table 5. The constructed BPNN-based particle identification model is shown in Fig. 7.

The training procedures of the wear particle classifier are described as follows [17]:

(1) Input training sample and randomly initialize the network parameters.
(2) Application of the forward propagation for the calculation of the output result layer-by-layer according to the weight matrix and input vectors.
(3) Calculate total output error E with Eq. (4).

$$E = \frac{1}{2}\sum_{k=1}^{l} e_k^2 = \frac{1}{2}\sum_{k=1}^{l}(d_k - o_k)^2, \quad (k = 1, 2, \ldots, l) \tag{4}$$

where d_k is the expected output value of kth node in the output layer, o_k is the real output value of kth node in the output layer, and l is the number of the node.
(4) Error back propagation to each layer and modify connection weights and thresholds to lower the gradient.

$$W_{jk}(t+1) = W_{jk}(t) - \xi\frac{\partial E}{\partial W_{jk}(t)}, \quad (j = 1, 2, \ldots, m;\ k = 1, 2, \ldots, l) \tag{5}$$

$$v_{jk}(t+1) = v_{jk}(t) - \xi\frac{\partial E}{\partial v_{jk}(t)}, \quad (j = 1, 2, \ldots, m;\ k = 1, 2, \ldots, l) \tag{6}$$

where ξ is the learning rate, v_{jk} is the weight value updating from jth node of the input layer to the kth node the hidden layer, and W_{jk} is the weight value from the jth node of the hidden layer to the kth node of the output layer.
(5) The determination as to whether or not the training process meets the termination condition: the error or the number of iterations reaches the set threshold. If not, start the next training with the second step.

3.4 Method Verification. In order to evaluate the performance of the constructed two-level classification model, the sample base in Ref. [24] is selected as the training and tested samples, including 54 particles of each type. There occurs the selection of 44 particle images from each type to train the constructed classification model and the rest is adopted as tested particles. Part of samples is illustrated in Fig. 8.

3.4.1 Wear Particle Recognition Based on Fuzzy Inference. The attributive degrees between tested particles and typical particles in the sample base are calculated by maximum–minimum proximity method, as shown in Fig. 9. The identification result is the type which corresponds to the highest point, and the final

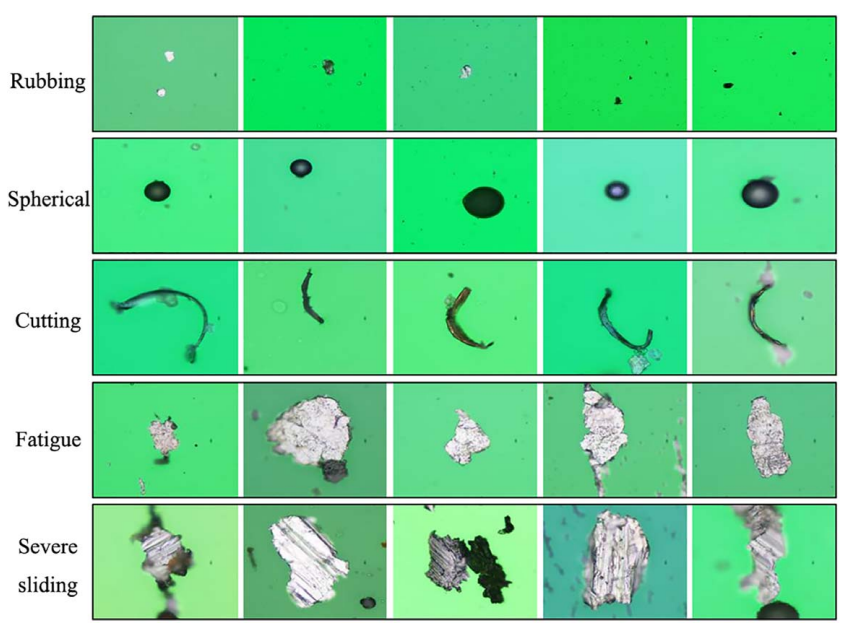

Fig. 8 Five types of wear particle samples

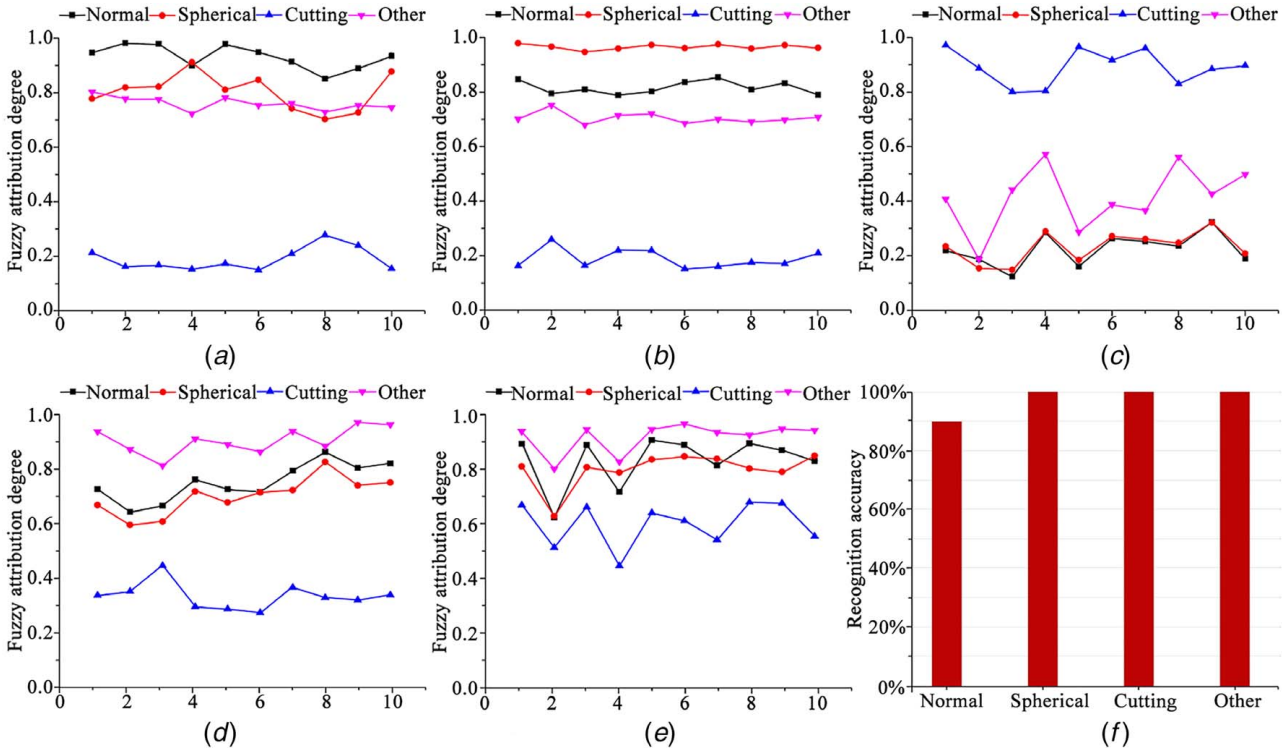

Fig. 9 Recognition results of tested particles based on fuzzy inference: (*a*) rubbing samples, (*b*) spherical samples, (*c*) cutting samples, (*d*) fatigue samples, (*e*) severe sliding samples, (*f*) recognition accuracy of particles (note: fatigue samples in (*d*) and severe sliding samples in (*e*) are grouped into the same category named "other particles")

recognition accuracy of all wear particles is calculated from Figs. 9(*a*)–9(*e*), as illustrated in Fig. 9(*f*). All particles are correctly identified except for a rubbing particle. The high recognition rate of rubbing, cutting, and spherical particles establishes a solid basis for the following two kinds of similar particle classification.

3.4.2 BPNN-Based Fatigue and Severe Sliding Particle Identification. With the comprehensive textures and constructed BPNN recognition method, 10 fatigue and severe sliding particles are tested, and the results are given in Tables 6 and 7. It may be observed that the identification rate of these two kinds of particles has reached 80%. Only No. 7 and No. 10 in tested fatigue samples and No. 4 and No. 8 in tested severe sliding samples have recognition errors. Compared with GLCM parameters or Tamura parameters, comprehensive texture parameters can effectively improve the recognition rate of these two kinds of particles. The accuracy comparison of different parameters is shown in Fig. 10.

4 Discussions

An automated WDA method is developed to analyze the wear particles generated from petrochemical equipment, involving the adaptive segmentation and identification of wear particles. The outcome of the experimental investigations have exposed the fact that the proposed automatic WDA strategy may be able to recognize rubbing, cutting, spherical, fatigue, and severe sliding particles with satisfactory accuracy. Compared with conventional techniques for particle identification, this newly proposed approach offers distinct advantages which are detailed below.

Compared with conventional 2D image-based identification algorithms [13,15], this proposed methodology clearly depicts the facilitation of the identification of wear particle types. When compared with the newly integrated strategy of BPNN and CNN method [24], the recognition rate of rubbing, cutting, and spherical particles has been over 90%. Although they have a similar accuracy in identifying the type of severe sliding and fatigue particles, our proposed method is constructed with BPNN, which have low

Table 6 Recognition results of fatigue particles

Particle	1	2	3	4	5	6	7	8	9	10
Fatigue	0.87	0.73	0.59	1.03	0.57	0.92	0.13	1.06	0.74	−0.10
Severe sliding	0.14	0.26	0.39	0.04	0.45	0.08	0.87	−0.07	0.26	1.11

Table 7 Recognition results of severe sliding particles

Particle	1	2	3	4	5	6	7	8	9	10
Fatigue	−0.05	−0.57	−0.06	0.96	0.22	0.40	0.47	0.74	0.18	0.16
Severe sliding	1.06	1.58	1.05	0.04	0.78	0.60	0.53	0.26	0.82	0.85

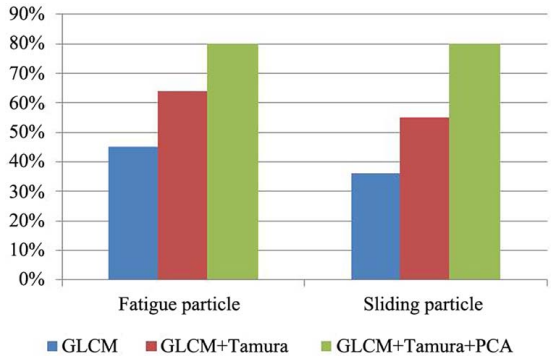

Fig. 10 Comparison of recognition accuracy of various parameters

hardware requirements for training the model. Although 3D imaging techniques have facilitated the identification of severe sliding and fatigue particles [18–20], the complexities involved in the operation and their high costs have greatly marginalized their application in industries. Hence, this constructed model can be considered as a practical approach for the identification of wear particle. Having successfully identified the particles, future work may now focus on the analysis of wear mechanisms for the full-life monitoring of petrochemical equipment.

5 Conclusions

In order to develop an automated ferrograph technology for petrochemical industries, a new method is established, including the adaptive segmentation and the two-level identification of wear particles. This proposed model is capable of classifying five typical particles produced from the petrochemical equipment. The main conclusions are that as follows:

(1) Extracted from RGB and HSV color space, three channel images can describe particles from different perspectives. With Otsu threshold method and image processing, particles in the dark, light, and mixed colors can be accurately segmented from the background.
(2) A fuzzy inference based classification algorithm is developed with three characteristic parameters (area, roundness, and aspect ratio). The estimated accuracy of the recognition on rubbing, cutting, and spherical particles is over 90%.
(3) In view of the limitation of the single-texture model in describing particle surfaces, three statistical texture parameters are calculated by applying PCA on seven textures from GLCM and Tamura textures. These parameters enable a BPNN classifier to be established for the classification of the fatigue and severe sliding particles. The average recognition accuracy of the two particles is 80%.

Acknowledgment

This research work is supported by the National Key R&D Program of China (No. 2018YFB1306100), the National Natural Science Foundation of China (Funder ID: 10.13039/501100001809) (No. 51675403 and No. 51975455), and the International Collaborative Plan of Shaanxi Province (No. 2017kw-034). The authors gratefully acknowledge the support of K.C. Wang Education Foundation.

References

[1] Kumar, M., Shankar Mukherjee, P., and Mohan Misra, N., 2013, "Advancement and Current Status of Wear Debris Analysis for Machine Condition Monitoring: A Review," Ind. Lubrication Tribol., **65**(1), pp. 3–11.
[2] Wang, S., Wu, T., Yang, L., Kwok, N., and Sarkodie-Gyan, T., 2019, "Three-Dimensional Reconstruction of Wear Particle Surface Based on Photometric Stereo," Measurement, **133**, pp. 350–360.
[3] Peng, Y., Cai, J., Wu, T., Cao, G., Kwok, N., Zhou, S., and Peng, Z., 2019, "Online Wear Characterisation of Rolling Element Bearing Using Wear Particle Morphological Features," Wear, **430**, pp. 369–375.
[4] Peng, Y., Cai, J., Wu, T., Cao, G., Kwok, N., Zhou, S., and Peng, Z., 2019, "A Hybrid Convolutional Neural Network for Intelligent Wear Particle Classification," Tribol. Int., **138**, pp. 166–173.
[5] Stachowiak, G., and Podsiadlo, P., 2006, "Towards the Development of An Automated Wear Particle Classification System," Tribol. Int., **39**(12), pp. 1615–1623.
[6] Feng, S., Qiu, G., Luo, J., Han, L., Mao, J., and Zhang, Y., 2019, "A Wear Debris Segmentation Method for Direct Reflection Online Visual Ferrography," Sensors, **19**(3), p. 723.
[7] Wang, J. Q., Yao, P. P., Liu, W. L., and Wang, X. L., 2016, "A Hybrid Method for the Segmentation of a Ferrograph Image Using Marker-Controlled Watershed and Grey Clustering," Tribol. Trans., **59**(3), pp. 513–521.
[8] Ma, M., and Zhao, L., 2014, "Research on Image Processing Technology for Online Oil Monitoring System," Proceedings of the IEEE International Conference on Imaging Systems and Techniques (IST), New York, Oct. 14–17.
[9] Wang, J., Zhang, L., Lu, F., and Wang, X., 2014, "The Segmentation of Wear Particles in Ferrograph Images Based on an Improved Ant Colony Algorithm," Wear, **311**(1–2), pp. 123–129.
[10] Memon, Q. A., and Laghari, M. S., 2005, "Self Organizing Analysis Platform for Wear Particle," Trans. Eng. Comput. Technol., **6**, pp. 122–125.
[11] Peng, P., and Wang, J., 2019, "Wear Particle Classification Considering Particle Overlapping," Wear, **422**, pp. 119–127.
[12] Wang, J., Bi, J., Wang, L., and Wang, X., 2018, "A Non-Reference Evaluation Method for Edge Detection of Wear Particles in Ferrograph Images," Mech. Syst. Signal Process., **100**, pp. 863–876.
[13] Yuan, W., Chin, K., Hua, M., Dong, G., and Wang, C., 2016, "Shape Classification of Wear Particles by Image Boundary Analysis Using Machine Learning Algorithms," Mech. Syst. Signal Process., **72**, pp. 346–358.
[14] Wu, T., Peng, Y., Sheng, C., and Wu, J., 2014, "Intelligent Identification of Wear Mechanism Via On-Line Ferrograph Images," Chin. J. Mech. Eng., **27**(2), pp. 411–417.
[15] Wang, J., and Wang, X., 2013, "A Wear Particle Identification Method by Combining Principal Component Analysis and Grey Relational Analysis," Wear, **304**(1–2), pp. 96–102.
[16] Xu, B., Wen, G., Zhang, Z., and Chen, F., 2018, "Wear Particle Classification Using Genetic Programming Evolved Features," Lubrication Sci., **30**(5), pp. 229–246.
[17] Wang, S., Wu, T., Shao, T., and Peng, Z., 2019, "Integrated Model of BP Neural Network and Cnn Algorithm for Automatic Wear Debris Classification," Wear, **426**, pp. 1761–1770.
[18] Tian, Y., Wang, J., Peng, Z., and Jiang, X., 2012, "A New Approach to Numerical Characterisation of Wear Particle Surfaces in Three-Dimensions for Wear Study," Wear, **282**, pp. 59–68.
[19] Stachowiak, G. P., Stachowiak, G. W., and Podsiadlo, P., 2008, "Automated Classification of Wear Particles Based on Their Surface Texture and Shape Features," Tribol. Int., **41**(1), pp. 34–43.
[20] Peng, Z., and Kirk, T., 1998, "Computer Image Analysis of Wear Particles in Three-dimensions for Machine Condition Monitoring," Wear, **223**(1–2), pp. 157–166.
[21] Otsu, N., 1979, "A Threshold Selection Method From Gray-Level Histograms," IEEE Trans. Syst. Man Cybernet., **9**(1), pp. 62–66.
[22] Peng, Y., Wu, T., Wang, S., and Peng, Z., 2015, "Oxidation Wear Monitoring Based on the Color Extraction of On-Line Wear Debris," Wear, **332**, pp. 1151–1157.
[23] Tan, K. S., Lim, W. H., and Isa, N. A. M., 2013, "Novel Initialization Scheme for Fuzzy C-means Algorithm on Color Image Segmentation," Appl. Soft Comput., **13**(4), pp. 1832–1852.
[24] Peng, Z., and Kirk, T., 1998, "Automatic Wear-Particle Classification Using Neural Networks," Tribol. Lett., **5**(4), pp. 249–257.
[25] Müller, T., Pór, A., and Sereni, J.-S., 2008, "Lower Bounding the Boundary of a Graph in Terms of Its Maximum Or Minimum Degree," Discrete Math., **308**(24), pp. 6581–6583.
[26] Bharati, M. H., Liu, J. J., and MacGregor, J. F., 2004, "Image Texture Analysis: Methods and Comparisons," Chemom. Intell. Lab. Syst., **72**(1), pp. 57–71.
[27] Tamura, H., Mori, S., and Yamawaki, T., 1978, "Textural Features Corresponding to Visual Perception," IEEE Trans. Syst. Man Cybernet., **8**(6), pp. 460–473.
[28] Fung, C.-P., and Kang, P.-C., 2005, "Multi-Response Optimization in Friction Properties of PBT Composites Using Taguchi Method and Principle Component Analysis," J. Mater. Process. Technol., **170**(3), pp. 602–610.
[29] Pan, L. K., Wang, C. C., Wei, S. L., and Sher, H. F., 2007, "Optimizing Multiple Quality Characteristics Via Taguchi Method-Based Grey Analysis," J. Mater. Process. Technol., **182**(1–3), pp. 107–116.
[30] Wong, W. K., Yuen, C., Fan, D., Chan, L., and Fung, E., 2009, "Stitching Defect Detection and Classification Using Wavelet Transform and BP Neural Network," Expert Syst. Appl., **36**(2), pp. 3845–3856.
[31] Zhao, B., Li, X., Lu, X., and Wang, Z., 2018, "A CNN-RNN architecture for multi-label weather recognition," Neurocomputing, **322**, pp. 47–57.